Evidence for an early wet Moon from experimental crystallization of the lunar magma ocean

Lin, Yanhao; Tronche, Elodie J.; Steenstra, Edgar S.; van Westrenen, Wim

published in
Nature Geoscience
2017

DOI (link to publisher)
10.1038/NGEO2845

document version
Publisher's PDF, also known as Version of record

ARTICLES
PUBLISHED ONLINE: 28 NOVEMBER 2016 | DOI: 10.1038/NGEO2845
nature geoscience

Evidence for an early wet Moon from experimental crystallization of the lunar magma ocean

Yanhao Lin*, Elodie J. Tronche, Edgar S. Steenstra and Wim van Westrenen*

The Moon is thought to have been covered initially by a deep magma ocean, its gradual solidification leading to the formation of the plagioclase-rich highland crust. We performed a high-pressure, high-temperature experimental study of lunar mineralogical and geochemical evolution during magma ocean solidification that yields constraints on the presence of water in the earliest lunar interior. In the experiments, a deep layer containing both olivine and pyroxene is formed in the first ∼50% of crystallization, β-quartz forms towards the end of crystallization, and the last per cent of magma remaining is extremely iron rich. In dry experiments, plagioclase appears after 68 vol.% solidification and yields a floatation crust with a thickness of ∼68 km, far above the observed average of 34–43 km based on lunar gravity. The volume of plagioclase formed during crystallization is significantly less in water-bearing experiments. Using the relationship between magma water content and the resulting crustal thickness in the experiments, and considering uncertainties in initial lunar magma ocean depth, we estimate that the Moon may have contained at least 270 to 1,650 ppm water at the time of magma ocean crystallization, suggesting the Earth–Moon system was water-rich from the start.

The magma ocean concept has been a cornerstone of lunar evolution models since the return of the first lunar samples[1,2]. A magma ocean stage is very likely if the Moon formed from the debris of a highly energetic collision between the Earth and another large planetary body[3,4]. Studies of early metallic core segregation in the Moon also suggest very high initial temperatures consistent with a deep magma ocean[5,6]. Crystallization of the lunar magma ocean (LMO) is thought to create a series of concentric cumulate layers with different chemical compositions and mineralogical assemblages, including an anorthositic crust via floatation of low-density plagioclase-rich cumulates[1,2,7]. The crystallization sequence and composition of cumulate layers drive subsequent events in lunar evolution, including the proposed buoyancy-driven overturn of the mantle leading to mare basalt volcanism, and prior studies have modelled magma ocean crystallization for a variety of ocean compositions and depths[2,8–10]. Most previous models (summarized in Fig. 1a–d) produce broadly similar cumulate assemblages, with Mg-rich olivine crystallizing first, followed by orthopyroxene, creating a dunite layer covered by harzburgite in the lower lunar mantle[2,10]. Anorthitic plagioclase begins to crystallize late (after >70 per cent solidification by volume, PCS), floating to the surface to form the primary lunar crust. Corresponding mafic cumulates become more Fe-rich as crystallization proceeds, and after >95 PCS a dense ilmenite-rich layer forms[2]. The final residual LMO dregs become enriched in potassium (K), rare earth elements (REE), and phosphorus (P), forming the source for KREEP-rich magmatic rocks[2,7,11].

These prior models were based on a limited set of high-pressure experiments, requiring numerical models to extrapolate to full magma ocean solidification. Most models ignored the effects of variable pressures within the molten ocean on crystallization. None of these models focused on the possible presence of water in the lunar interior at any stage of its evolution, as they predated the discovery of water in lunar samples. Since around 2008, the traditional view of a dry Moon[12] has been challenged by the identification of water in lunar pyroclastic glasses[13], lunar minerals including apatite[14–16] and melt inclusions in lunar olivine[17,18]. Water could therefore play an important role in the evolution of the Moon, including during the crystallization of the LMO[16].

Experiments to simulate magma solidification

We performed high-pressure, high-temperature experiments to simulate LMO crystallization in dry and water-bearing conditions, in the system Ca-Fe-Mg-Al-Ti-Si-O (CFMATS). We assume an initial LMO depth of 700 km, in the middle of the range of current estimates between 400 and 1,000 km (ref. 19). The starting composition, based on geophysical data for the Moon[20], is slightly lower in aluminium abundance and higher in iron abundance than the lunar primitive upper mantle (LPUM) composition used for the oft-cited LMO numerical model of Snyder *et al.*[2], and has the same aluminium content as the bulk silicate earth[21] (Supplementary Table 1). During each step of LMO crystallization, the effects of pressure in the molten ocean on magma crystallization were taken into account explicitly. We assume that as a result of convection, the lunar magma ocean is isothermal. In each step, we performed several isothermal experiments at the range of pressures covering the depth of the ocean in that particular step. This mimics the behaviour of a real-world magma ocean, in that the deepest parts of the magma generally produce the highest proportion of crystallizing phases. Details of starting material synthesis and experimental conditions are given in the Methods and Supplementary Information, respectively.

Solidification of a dry magma ocean

Results of our crystallization experiments are summarized in Table 1 and Supplementary Table 2, and in Fig. 1e,f. In a dry LMO (Fig. 1e), olivine (Fo_{97-88}) and low-Ca pyroxene ($En_{88-85}Fs_{12-10}Wo_{1-3}$; referred to as Opx hereafter) crystallize together as the first assemblage phase, with the Opx/olivine ratio decreasing at shallower levels in this initial LMO. As crystallization proceeds and the bottom of the remaining LMO shallows upon cooling, Opx is

Faculty of Earth and Life Sciences, VU Amsterdam, De Boelelaan 1085, 1081 HV Amsterdam, The Netherlands. *e-mail: y.lin@vu.nl; w.van.westrenen@vu.nl

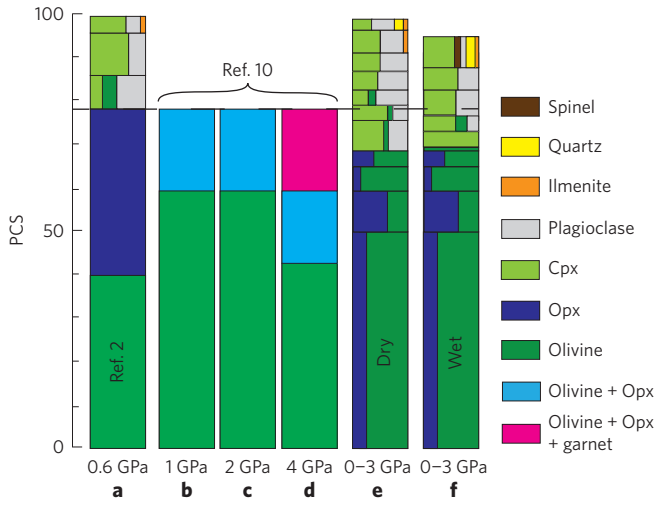

Figure 1 | Comparison of LMO crystallization sequences from this study and the literature. a, Numerically determined crystallization sequence[2]. **b**–**d**, Experimentally determined crystallization sequences up to 78 PCS (per cent solid by volume) for the LPUM bulk Moon compositions at 1, 2 and 4 GPa (ref. 10). **e**,**f**, Experiments for a dry system (**e**) and a system containing 3,150 ppm water (**f**) in a LMO with initial depth of 700 km. Cpx, clinopyroxene; Opx, orthopyroxene.

replaced by Ca-bearing pyroxene ($En_{76-49}Fs_{39-18}Wo_{6-12}$; referred to as Cpx hereafter). The appearance of Cpx is almost simultaneous with that of plagioclase at 1,240 °C in a dry LMO. The crystallizing assemblage of coexisting olivine and Opx is replaced by olivine, Cpx and plagioclase from 68 to 83 PCS. Subsequently, olivine disappears. Ilmenite starts forming from 91 PCS. We found β-quartz, a phase that was not observed in previous LMO crystallization models, starts forming at 1,100 °C and 0.4 GPa. Due to its low density it is expected to float towards the bottom of the plagioclase crust. Ferroan anorthosites in the lunar sample collection are typically poor in quartz, instead containing significant proportions of olivine[22]. In our experiments, early formed plagioclase coexists with olivine. This suggests that older LMO plagioclase grains (including some olivine) form the top of the lunar crust, whereas younger quartz-rich plagioclase cumulates may be hidden in deeper crustal sections. Overall cumulate layer density increases with decreasing depth. This gravitationally unstable configuration eventually leads to an overturn of the lunar mantle after completion of LMO solidification[2,23].

The MgO content and Mg# (molar Mg/(Mg + Fe)) of the residual magma decrease continuously as crystallization progresses (Supplementary Table 2). SiO_2 increases gradually with minor fluctuations until 96 PCS, and then decreases sharply with the occurrence of β-quartz. Magma CaO and Al_2O_3 increase steadily to maxima of 11.4 wt% and 15.8 wt% around 80 PCS, respectively, after which plagioclase and Cpx appear. The appearance of ilmenite at 91 PCS significantly affects the shape of the curves for the TiO_2 and FeO concentrations. In sharp contrast to the calculations of Snyder *et al.*[2], magma FeO shows extreme enrichment in the final crystallization steps, ending at >26 wt%.

Figure 1e shows a comparison of the dry crystallization sequence of this study compared to the dry models of Snyder *et al.*[2] and Elardo *et al.*[10] (Fig. 1a–d). The Snyder *et al.* model[2] did not consider the full range of applicable LMO pressure regimes and assumed a 78 PCS equilibrium cutoff, and the Elardo model[10] gave experiment results only up to 78 PCS with a 50 PCS equilibrium cutoff under a limited set of pressure conditions. Because Elardo *et al.*[10] focused on early LMO evolution, their study did not yield plagioclase, ilmenite or quartz. Figure 1 shows the significant differences in crystallized sequences with these previous studies, including a different deep cumulate mineralogy, earlier formation of plagioclase, and late formation of quartz.

A clear discrepancy with observations

The thickness of the lunar crust (consisting of plagioclase and quartz) resulting from the solidification of a dry LMO is 67.5 km at 99 PCS, assuming full segregation of both phases (Fig. 2). This is far greater than observed based on the recent GRAIL gravity field mission to the Moon[24] which constrains average crustal thickness to 34–43 km. Changing the assumed bulk composition of the LMO would affect the resulting crustal thickness. The aluminium content of our starting composition (4.5 wt% Al_2O_3) is close to that of the bulk silicate earth (BSE, 4.4 wt% Al_2O_3), and is mildly enriched in iron, conforming to current thinking about similarities in composition between the Moon and the BSE (Supplementary Table 1). The large mismatch in crustal thickness between our experiments and gravity-based observations develops despite the fact that the aluminium content of our bulk composition, which correlates with the potential for plagioclase formation, is lower than most lunar composition models (Supplementary Table 1). The Al_2O_3 concentration in the Moon required to yield a crustal thickness of less than 43 km would be <3.0 wt%, a value that is far below all current lunar compositional models (Supplementary Table 1).

Imperfect segregation of plagioclase and quartz to the lunar crust would yield a thinner crust (as part of the plagioclase and/or quartz produced would remain in the lunar mantle), but the efficiency of segregation would have to be unrealistically low to explain the large discrepancy. Finally, crustal thickness depends on the assumed initial depth of the magma ocean. Assuming no Al-rich phase solidifies at high pressure, total crustal thickness based on thermodynamic modelling[25] is >70 km if the initial dry LMO depth is 1,000 km, and ~52 km for a 400-km-deep dry LMO. Overall, even when considering these uncertainties, it is clear that crystallization of a dry LMO leads to a lunar highland crust that is significantly thicker than observed.

The effect of water on magma ocean solidification

This major discrepancy can be solved by incorporating the effect of the presence of water in the Moon at the time of LMO crystallization. Experimental studies of terrestrial magmatism have previously shown that water addition inhibits the crystallization of plagioclase with respect to crystallization of more mafic phases (pyroxene and olivine)[26]. The effect of water addition on lunar crustal thickness was quantified by performing fractional crystallization experiments of two wet LMO compositions by adding 0.5 and 1.0 wt% H_2O, respectively, to the melt composition that yielded the first plagioclase crystals in dry experiments (step LBS5, Table 1). This approach is equivalent to adding 1,575 and 3,150 ppm water to a 700-km-deep magma ocean, assuming water does not significantly affect the olivine/opx ratio during the earlier crystallization steps[26]. At our experimental conditions, the $H_2/(H_2+H_2O)$ ratio is small (0.1–0.3), as expected for the Moon[27], and we report all water as H_2O. In all subsequent crystallization steps, water loss from the LMO was assumed to be minimal (that is, we assumed no significant degassing of water from the Moon occurred during LMO crystallization), leading to an increase in the water content of the residual magma with each crystallization step. Results of wet experiments are summarized in Table 1, and the mineralogy of a solidified LMO initially containing 3,150 ppm water is shown in Fig. 1f. Consistent with data from terrestrial systems[26], wet crystallization experiments show a delay in the appearance of plagioclase. At 1,575 and 3,150 ppm water, plagioclase appears after 71 and 73 PCS, respectively, compared to 68 PCS in the dry system. The total amount of plagioclase also decreases with increasing water content, with Al substituting into pyroxene and spinel[26].

Table 1 | Summary of experimental results.

		No water				1,575 ppm water				3,150 ppm water		
Dry exp. step	*T* (°C)	Mineral assemblage (vol.%)	PCS	FCT (km)	Wet exp. step	Mineral assemblage (vol.%)	PCS	FCT (km)		Mineral assemblage (vol.%)	PCS	FCT (km)
			0	0								
LBS1	1550	83% olivine$_{(Fo_{97-88})}$ + 17% pyroxene ($En_{88-85}Fs_{12-10}Wo_{1-3}$)										
			49.6	0								
LBS2	1400	36% olivine$_{(Fo_{88-86})}$ + 64% pyroxene ($En_{86-85}Fs_{13-11}Wo_{2-3}$)										
			60.0	0								
LBS3	1340	92% olivine$_{(Fo_{87-86})}$ + 8% pyroxene ($En_{85}Fs_{12}Wo_3$)										
			63.8	0								
LBS4	1280	59% olivine$_{(Fo_{87-82})}$ + 41% pyroxene ($En_{82-80}Fs_{16-15}Wo_{3-4}$)										
			68.5	0			68.5	0			68.5	0
LBS5	1240	11% olivine$_{(Fo_{83})}$ + 55% pyroxene ($En_{75-74}Fs_{19}Wo_6$) + 34% plagioclase			LBS5H	10% olivine$_{(Fo_{83})}$ + 90% pyroxene ($En_{81-80}Fs_{17-16}Wo_{4-3}$)				Olivine$_{(Fo_{83})}$		
			76.1	12.3			71.6	0			69.6	0
LBS6	1220	10% olivine$_{(Fo_{81})}$ + 60% pyroxene ($En_{76-69}Fs_{21-18}Wo_{10-6}$) + 30% plagioclase			LBS6H	32% olivine$_{(Fo_{80-78})}$ + 45% pyroxene ($En_{76-73}Fs_{20}Wo_{7-4}$) + 23% plagioclase				Pyroxene ($En_{79-75}Fs_{18-17}Wo_{7-4}$)		
			79.3	16.8			75.8	4.5			73.3	0
LBS7	1200	10% olivine$_{(Fo_{79})}$ + 30% pyroxene ($En_{76-75}Fs_{19-18}Wo_6$) + 60% plagioclase			LBS7H	59% pyroxene ($En_{73-71}Fs_{22-21}Wo_{7-6}$) + 41% plagioclase				20% olivine $_{(Fo_{81})}$ + 60% pyroxene ($En_{78-77}Fs_{19-18}Wo_4$) + 20% plagioclase		
			82.8	26.5			81.0	14.6			76.8	3.2
LBS8	1180	42% pyroxene ($En_{71}Fs_{22}Wo_7$) + 58% plagioclase			LBS8H					60% pyroxene ($En_{66-63}Fs_{25-24}Wo_{12-10}$) + 40% plagioclase		
			87.2	39.0							82.6	14.1
LBS9	1160	50% pyroxene ($En_{70}Fs_{24}Wo_6$) + 50% plagioclase			LBS9H					62% pyroxene ($En_{60}Fs_{28}Wo_{12}$) + 38% plagioclase		
			91.1	48.0							88.5	24.9
LBS10	1130	50% pyroxene ($En_{63}Fs_{31}Wo_6$) + 45% plagioclase + 5% Ilmenite			LBS10H					56% pyroxene ($En_{35}Fs_{31}Wo_{34}$) + 9% plagioclase + 7% Ilmenite + 17% Quartz + 11% Spinel		
			96.4	60.2							94.7	32.2*
LBS11	1100	33% pyroxene ($En_{49}Fs_{39}Wo_{12}$) + 39% plagioclase + 12% Ilmenite + 16% Quartz										
			99.0	67.5*								

*Including quartz; FCT, Floating crustal thickness (100% plagioclase); exp. experiment; PCS, per cent solid by volume. At PCS = 99.0, the calculated crustal thickness is 42 km (s.d. = 1.13) at 1,575 ppm water, and 40 km (s.d. = 1.28) at 3,150 ppm water, respectively.

Water in the Earth–Moon system

The net effect of adding water on the resulting crustal thickness at 99 PCS is nonlinear, as summarized in Fig. 2. Adding 1,575 ppm water to an initially 700-km-deep LMO decreases final crustal thickness from 67.5 to 42 km, within the GRAIL range, while addition of 3,150 ppm water addition yields a crust of 40 km. We estimated the effect of water addition to magma oceans of 400 or 1,000 km initial depth assuming the same fractional decrease

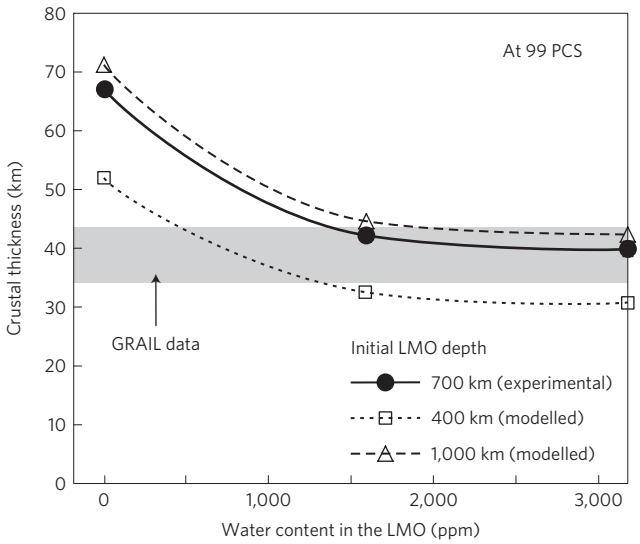

Figure 2 | Average thickness of the lunar crust as a function of initial LMO water content. Filled circles and solid line show experimental results from this study; triangles and squares connected by dashed/dotted lines show crustal thickness curves assuming different LMO depths calculated using thermodynamic modelling[25]. Grey bar shows observed average crustal thickness of 34–43 km based on GRAIL data[24].

in plagioclase production with water content as measured in our experiments (Fig. 2). By combining our dry and wet results we estimate that the LMO must have contained at least 500 ppm water to yield the crustal thickness observed by GRAIL if the LMO was shallow, and >1,800 ppm water if the LMO was deep (Fig. 2). This translates to water abundances in the whole Moon (assuming all rocks underneath the bottom of the magma ocean were devoid of water) of at least 270–1,650 ppm water at the time of LMO crystallization, with deeper initial magma oceans necessitating a wetter Moon. Additional experiments further quantifying the effects of LMO depth and LMO composition can improve these estimates.

Inefficient segregation of plagioclase and quartz would yield a thinner crust (lowering the amount of water required). On the other hand, although we have taken utmost care to minimize the amount of water in our dry experiments (see Methods), our nominally anhydrous experiments could contain up to ~0.05 wt% water[28], equivalent to having ~160 ppm water in the initial magma ocean. If this were the case, the minimum amount of water required to explain the observed lunar crustal thickness would increase by up to 20%. Finally, we reiterate that our wet experimental series assume no degassing took place during LMO crystallization. As a result, the water content of the magma increases with progressive crystallization. Interpretations of volatile contents of lunar samples often invoke (the possibility of) degassing[13,29]. To first order, if the later stages of LMO crystallization occurred in a water-poor environment due to degassing, earlier stages must have been characterized by even higher water contents than estimated based on our experiments, to yield an overall crustal thickness consistent with observations. There may be multiple pathways to reach a final crustal thickness of 34–43 km, but all of them involve the presence of water during LMO crystallization.

The estimated lower bound on lunar interior water content is consistent with a single study of the measured water content of plagioclase in lunar highland samples[16], but water contents of the lunar interior based on analyses of samples that postdate the LMO stage[13,14,17] generally yield much lower values. This suggests that the Moon was wet from the start, and that significant water was subsequently lost from the lunar interior, through degassing either during or after the magma ocean stage. A wet start of the Moon, coupled with the strong similarities between the composition of the Moon and the composition of the silicate Earth, suggests that equally high concentrations of water were present in the Earth at the time of the Moon-forming event[3,4].

Methods

Methods, including statements of data availability and any associated accession codes and references, are available in the online version of this paper.

Received 27 May 2016; accepted 27 October 2016; published online 28 November 2016

References

1. Warren, P. H. The magma ocean concept and lunar evolution. *Annu. Rev. Earth Planet. Sci.* **13,** 201–240 (1985).
2. Snyder, G. A., Taylor, L. A. & Neal, C. R. A chemical model for generating the sources of mare basalts: combined equilibrium and fractional crystallization of the lunar magmasphere. *Geochim. Cosmochim. Acta* **56,** 3809–3823 (1992).
3. Ćuk, M. & Stewart, S. T. Making the Moon from a fast-spinning Earth: a giant impact followed by resonant despinning. *Science* **338,** 1047–1052 (2012).
4. Canup, R. M. Forming a Moon with an Earth-like composition via a giant impact. *Science* **338,** 1052–1055 (2012).
5. Rai, N. & Van Westrenen, W. Lunar core formation: new constraints from metal-silicate partitioning of siderophile elements. *Earth Planet. Sci. Lett.* **388,** 343–352 (2014).
6. Steenstra, E. S., Rai, N., Knibbe, J. S., Lin, Y. H. & van Westrenen, W. New geochemical models of core formation in the Moon from metal-silicate partitioning of 15 siderophile elements. *Earth Planet. Sci. Lett.* **441,** 1–9 (2016).
7. Shearer, C. K. *et al*. Thermal and magmatic evolution of the Moon. *Rev. Mineral. Geochem.* **60,** 365–518 (2006).
8. Longhi, J. A. Model of early lunar differentiation. *Proc. Lunar Planet. Sci. Conf.* **11,** 289–315 (1980).
9. Tonks, W. B. & Melosh, H. J. *Origin of the Earth* (Oxford Univ. Press, 1990).
10. Elardo, S. M., Draper, D. S. & Shearer, C. K. Lunar magma ocean crystallization revisited: bulk composition, early cumulate mineralogy, and the source regions of the highlands Mg-suite. *Geochim. Cosmochim. Acta* **75,** 3024–3045 (2011).
11. Warren, P. H. & Wasson, J. T. The origin of KREEP. *Rev. Geophys. Space Phys.* **17,** 73–88 (1979).
12. Taylor, S. R., Taylor, G. J. & Taylor, L. A. The Moon: a Taylor perspective. *Geochim. Cosmochim. Acta* **70,** 5904–5918 (2006).
13. Saal, A. E. *et al*. Volatile content of lunar volcanic glasses and the presence of water in the Moon's interior. *Nature* **454,** 192–195 (2008).
14. McCubbin, F. M. *et al*. Nominally hydrous magmatism on the Moon. *Proc. Natl Acad. Sci. USA* **107,** 11223–11228 (2010).
15. Boyce, J. W. *et al*. Lunar apatite with terrestrial volatile abundances. *Nature* **466,** 466–469 (2010).
16. Hui, H., Peslier, A. H., Zhang, Y. & Neal, C. R. Water in lunar anorthosites and evidence for a wet early Moon. *Nat. Geosci.* **6,** 177–180 (2013).
17. Hauri, E. H., Weinreich, T., Saal, A. E., Rutherford, M. C. & Van Orman, J. A. High pre-eruptive water contents preserved in lunar melt inclusions. *Science* **333,** 213–215 (2011).
18. Chen, Y. *et al*. Water, fluorine, and sulfur concentrations in the lunar mantle. *Earth Planet. Sci. Lett.* **427,** 37–46 (2015).
19. Elkins-Tanton, L. T., Burgess, S. & Yin, Q. Z. The lunar magma ocean: reconciling the solidification process with lunar petrology and geochronology. *Earth Planet. Sci. Lett.* **304,** 326–336 (2011).
20. Khan, A., Connolly, J. A. D., Maclennan, J. & Mosegaard, K. Joint inversion of seismic and gravity data for lunar composition and thermal state. *Geophys. J. Int.* **168,** 243–258 (2007).
21. McDonough, W. F. & Sun, S. S. The composition of the Earth. *Chem. Geol.* **120,** 223–253 (1995).
22. Steele, I. M. & Smith, J. V. Mineralogy and petrology of some Apollo 16 rocks and fines: general petrologic model of Moon. *Geochim. Cosmochim. Acta* **1,** 519–536 (1973).
23. De Vries, J., van den Berg, A. & van Westrenen, W. Formation and evolution of a lunar core from ilmenite-rich magma ocean cumulates. *Earth Planet. Sci. Lett.* **292,** 139–147 (2010).
24. Wieczorek, M. A. *et al*. The crust of the Moon as seen by GRAIL. *Science* **339,** 671–675 (2013).
25. Davenport, J. D., Longhi, J., Neal, C. R., Jolliff, B. J. & Bolster, D. Simulating planetary igneous crystallization environments (SPICEs): a suite of igneous crystallization programs. *Lunar Planet. Sci. Conf.* **45,** abstr. 1111 (2014).

26. Sisson, T. W. & Grove, T. L. Experimental investigations of the role of H_2O in calc-alkaline differentiation and subduction zone magmatism. *Contrib. Mineral. Petrol.* **113,** 143–166 (1993).
27. Hirschmann, M. M., Withers, A. C., Ardia, P. & Foley, N. T. Solubility of molecular hydrogen in silicate melts and consequences for volatile evolution of terrestrial planets. *Earth Planet. Sci. Lett.* **345–348,** 38–48 (2012).
28. Médard, E., McCammon, C. A., Barr, J. A. & Grove, T. L. Oxygen fugacity, temperature reproducibility, and H_2O contents of nominally anhydrous piston-cylinder experiments using graphite capsules. *Am. Mineral.* **93,** 1838–1844 (2008).
29. Tartèse, R. *et al*. Apatites in lunar KREEP basalts: the missing link to understanding the H isotope systematics of the Moon. *Geology* **42,** 363–366 (2014).

Acknowledgements

We thank S. Matveev and T. Bouten for technical assistance on electron microprobe analyses and B. Lacet for sample preparation. P. Warren is thanked for constructive criticisms. This work was supported by a Netherlands Organization for Scientific Research (N.W.O.) Vici award to W.v.W. and a China Scholarship Council fellowship to Y.L.

Author contributions

W.v.W., E.J.T. and Y.L. designed the project. Y.L. and E.J.T. performed the experiments. Y.L., E.J.T. and E.S.S. performed sample analyses. All authors discussed the results. Y.L. and W.v.W. wrote the paper with input from all authors.

Additional information

Supplementary information is available in the online version of the paper. Reprints and permissions information is available online at www.nature.com/reprints. Correspondence and requests for materials should be addressed to Y.L. or W.v.W.

Competing financial interests

The authors declare no competing financial interests.

Methods

Experimental design. The initial depth of the magma ocean was taken to be 700 km, well within the estimated range of 500–1,000 km (ref. 19). Supplementary Table 1 shows a comparison between the bulk composition of the LMO chosen for this study, other LMO crystallization studies, and the Bulk Silicate Earth[21]. The process of LMO crystallization was investigated by adopting a 'two-stage' model, with equilibrium crystallization persisting until 50 per cent solidification (PCS) based on calculations of the ability of suspending crystals in a cooling and convecting magma ocean[9]. We used a stepwise experimental approach for fractional crystallization of the LMO (Supplementary Table 2), with starting materials for the second step based on the composition of the residual liquid of the first crystallization step with removal of the corresponding crystals.

The depth of the residual LMO is based on a calculation of the increasing radius of solid material accumulating on the bottom of the magma ocean. The volume and composition of the cumulate pile and residual LMO for each step are calculated and weighed proportionally. Because of the spherical shape of the Moon, crystallization occurring in deeper parts of the LMO contributes less volumetrically than crystallization at shallow levels. Each crystallization step was performed at 1 to 7 different pressures, depending on the remaining depth of the magma ocean, and at as many temperatures as required to approach the targeted crystallization percentage.

Starting materials. Dry and wet starting materials were prepared by mixing appropriate amounts of high-purity (99.5–99.99%, Alfa Aesar) powdered (hydr)oxides (MgO, $Mg(OH)_2$, Fe_2O_3, Al_2O_3, $Al(OH)_3$, TiO_2, SiO_2) and $CaCO_3$ (99.95–100.05%, Alfa Aesar). The oxides MgO, Al_2O_3, TiO_2 and SiO_2 were fired overnight at 1,000 °C and then stored at 110 °C. The other oxides, hydroxides and calcium carbonate were dried at 110 °C overnight prior to use. After mixing nominally dry starting materials under ethanol in an agate mortar for 1 h, they were dried in air and decarbonated in a Pt crucible in a box furnace by gradually raising the temperature from 650 to 1,000 °C in approximately 7 h. The Pt crucible had previously been iron-saturated to minimize iron loss. The resulting mixtures were melted for 20 min at 1,500 °C to promote homogeneity. They were quenched by immersing the bottom of Pt crucible in water. Small fragments of all resulting glasses were embedded in epoxy, polished, carbon-coated and analysed for homogeneity by electron microprobe. The glasses were subsequently crushed, dried, and reground under ethanol in an agate mortar for 1 h, and then kept at 110 °C until use. For water-bearing experiments, water was added to dry glass using $Mg(OH)_2$ or $Al(OH)_3$.

High-pressure experiments. High-pressure, high-temperature experiments were performed in a piston cylinder press using a half-inch (12.7 mm) diameter talc-Pyrex cell assembly[30]. For these experiments a hand-machined graphite bucket, with an inner diameter of 0.7 mm, outer diameter of ~1.7 mm and a length of 3–4 mm, was filled with starting material, closed with a graphite lid and inserted in a Pt capsule, with an inner diameter of 1.7 mm, outer diameter of 2 mm, and a length of 5–7 mm. The bottom of the Pt capsule was triple-crimped, flattened and welded shut at one end. After inserting the graphite capsule, the other end was crimped and welded shut. For the dry experiments, capsules were held at 575 °C for ~10 min before closing and welding shut, to drive off residual moisture. The oxygen fugacity is around 1.1 log units below the iron-wüstite buffer in this assembly, so that iron is present in the 2^+ valence state. Temperature was monitored using a $W_{97}Re_3$–$W_{75}Re_{25}$ (type D) thermocouple and Eurotherm 2404 or Omega CN76000 programmable controller. The centre of the sample was located in the hotspot of the assembly, 2 mm away from the thermocouple tip end, so that sample temperatures were within 10 °C of the thermocouple reading[31]. Experiments were pressurized cold and then heated while maintaining pressure. Pressures range from 0.4 to 3 GPa and temperatures from 1,100 to 1,550 °C. Experiments at 1 atm were run in a high-temperature box furnace (temperatures between 1,200 and 1,550 °C). Experiment duration varied between 2 and 100 h, depending on the melting degree and temperature. At completion of an experiment, runs were quenched by cutting power to the heater, and the temperature typically dropped below the glass transition in <10 s.

Analytical techniques. Experimental run products were mounted in epoxy and polished for back-scattered electron (BSE) imagery used to assess the texture and mineralogy, and then carbon-coated for electron microprobe analysis (EMPA). The chemical composition of the run product phases (minerals and quenched melts) was determined using a JEOL JXA-8800M Electron Microprobe at Utrecht University, and checked for contamination and iron loss. Analysis were done using an accelerating voltage of 15 kV and a beam current of 20 nA for Si, Ti, Al, Fe, Mg and Ca. The mineral and melt proportions were determined by mass balance calculations and area percentage using an EDAX-EDS system in imaging mode. We used three different focused beams of 1, 10 and 20 μm diameter for the mineral phases, glassy quenched melts nearly free of quench crystals, and quenched melts, respectively. Analyses were calibrated against primary standards of diopside (Ca, Si), fayalite (Fe), ilmenite (Ti), olivine (Mg) and orthoclase (Al). Peak areas were converted to concentrations using standard values. Peak count times were 20 s and background count time 10 s. Compositions reported here are based on the average of 5–10 analyses. EMPA analyses of all glasses in the water-bearing experiments show totals that are significantly smaller than 100 per cent, correlating with the expected abundance of water derived from mass balance calculations, indicating water was retained during the experiments.

Demonstration of equilibrium. Texturally, mineral-melt contacts are straight without resorption textures. Low standard deviations for individual phase analyses in each experiment show that mineral grains are homogeneous in composition. Olivine–liquid Fe–Mg exchange coefficients, K_D, corrected for the effects of temperature, pressure and composition[32] vary from 0.24 to 0.30, well within the equilibrium value range of 0.17–0.45 (ref. 32). The average K_D^{Fe-Mg} values for pyroxene ranges from 0.23 to 0.41 except for one experiment at 1,100 °C (0.11), which is consistent with the equilibrium value range of 0.20–0.40 (refs 26,33,34).

Calculation of crustal thickness at 99 PCS in water-bearing systems. In all three experimental series, strong linear trends are observed when plotting crustal thicknesses (CT) derived from our experiments (based on the production of plagioclase + quartz) against LMO per cent solidification (PCS):

In the nominally dry system, $CT = 2.29 \times PCS - 161$ ($R^2 = 0.99$);

At 1,575 ppm water in the initial LMO, $CT = 1.57 \times PCS - 113$ ($R^2 = 0.98$);

At 3,150 ppm water in the initial LMO, $CT = 1.58 \times PCS - 117$ ($R^2 = 0.99$);

Based on these trends, at 99 PCS, CT is calculated to be 66 km in the dry system (in excellent agreement with the thickness of 67.5 km based on the 99 PCS dry experiments), 42 km at 1,575 ppm water, and 40 km at 3,150 ppm water. These are the thicknesses plotted in Fig. 2.

Code availability. The code used to generate the thermodynamic models shown in Fig. 2 is readily available at the Lunar and Planetary Institute website, http://www.lpi.usra.edu/lunar/tools/crystallizationcalculation.

Data availability. The authors declare that all relevant data supporting the findings of this study are available within the article and its Supplementary Information files, or available upon request from the corresponding author.

References

30. van Kan Parker, M., Mason, P. R. D. & van Westrenen, W. Experimental study of trace element partitioning between lunar orthopyroxene and anhydrous silicate melt: effects of lithium and iron. *Chem. Geol.* **285,** 1–14 (2011).
31. Watson, E. B., Wark, D., Price, J. D. & Van Orman, J. A. Mapping the thermal structure of solid-media pressure assemblies. *Contrib. Mineral. Petrol.* **142,** 640–652 (2002).
32. Toplis, M. J. The thermodynamics of iron and magnesium partitioning between olivine and liquid: criteria for assessing and predicting equilibrium in natural and experimental systems. *Contrib. Mineral. Petrol.* **149,** 22–39 (2005).
33. Grove, T. L. & Bryan, W. B. Fractionation of pyroxene-phyric MORB at low-pressure: An experimental-study. *Contrib. Mineral. Petrol.* **84,** 293–309 (1983).
34. Kinzler, R. J. & Grove, T. L. Primary magmas of mid-ocean ridge basalts 1. Experiments and methods. *J. Geophys. Res.* **97,** 6885–6906 (1992).